Transverse Modal Analysis of Printed Circuit Transmission Lines

HUNG-YUET YEE, SENIOR MEMBER, IEEE

Abstract—**Dispersion characteristics of finned rectangular waveguides, finlines, shielded slotlines, shielded microstrip and striplines, and shielded two-coupled slotlines and striplines are formulated by the transverse modal analysis method. A rectangular cavity is formed by placing two electric walls transverse to a uniform transmission-line system. Considering that the wave propagation is in the direction transverse to the transmission line and to the dielectric discontinuities, the rectangular cavity can be viewed as multiple rectangular waveguide sections joined by the discontinuities. The rectangular waveguide modal analysis technique is readily applicable to obtain the dispersion characteristics by matching the boundary conditions at the discontinuities interface. Numerical solutions are obtained using Galerkin's method, and the results are compared with several numerical techniques for various transmission-line systems.**

I. Introduction

SCATTERINGS from waveguide irises using the modal analysis technique have been investigated by Lee *et al.* [1] and Mittra *et al.* [2]. It is of interest to note that the numerical convergence depends on the ratio of the number of waveguide modes to the iris modes when the Galerkin's method is employed to obtain the numerical solutions. This technique is applicable to the transverse conducting strip in a rectangular waveguide and the convergence characteristics are similar to the waveguide iris solution. Taking advantage of the simplicity of the rectangular waveguide modal analysis, printed circuit transmission-line systems will be treated in this paper. This technique is well suited for the computation of practical narrow strips or slotlines where only a small determinant is required. Closed-form approximated equations can be derived for obtaining the physical insight to the solutions.

The orthogonal mode theory has been applied to ridge waveguide studies first by Collin and Daly [3] and then by Montgomery [4]. Their approach is similar to the present slotline formulation. The finline discontinuites are analyzed by Sorrentino and Itoh [5] using the transverse resonance method, which is similar to the techniques discussed in this paper. However, the emphasis here is on the numerical accuracy and the applications to various printed circuits transmission-line systems. The application of the transverse modal analysis to study microstrips and suspended-substrate striplines has not been reported in the literature. To simplify the presentation, stripline is understood to represent suspended-substrate stripline throughout this paper.

The following formulation is applicable to rectangular cavities with planar discontinuities. For shielded slotlines or striplines, a rectangular cavity can be formed by placing two electric walls transverse to the transmission line as shown in Figs. 1 and 2. Considering that the propagation is transverse to the slotline or stripline, the cavity can be recognized as multiple rectangular waveguide sections joined by the slotlines or striplines. A determinant, which is a function of frequency, can be derived by the modal analysis method. Slotline and stripline dispersion solutions are determined by cavity resonant frequencies which can be computed by setting the determinant equal to zero.

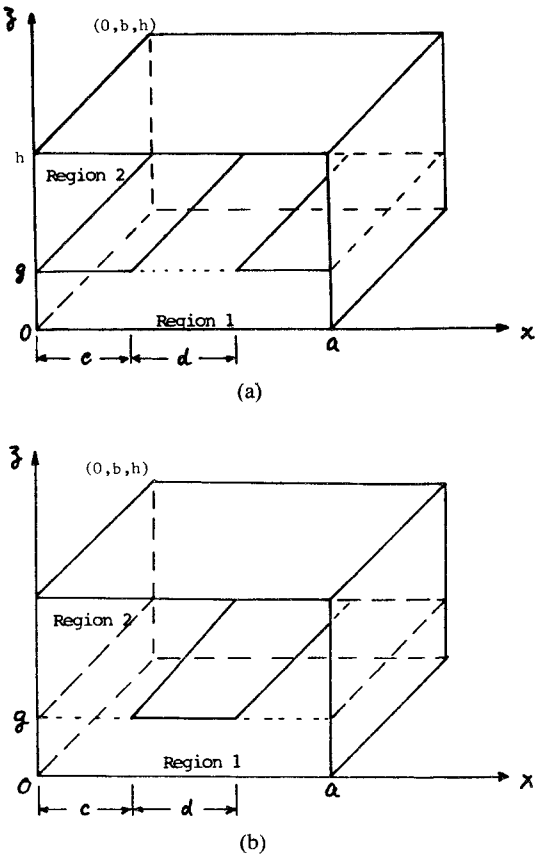

Fig. 1. Schematic diagram of two dielectric layer cavity. (a) Finline. (b) Shielded microstrip.

Equations derived in this paper are applicable to the following transmission-line systems:

1) finned rectangular waveguides,
2) finlines and shielded slotlines,
3) shielded microstriplines and striplines, and
4) shielded two broadside- or offset-coupled slotlines and striplines.

Manuscript received February 19, 1985; revised May 1, 1985.
The author is with the Antenna Laboratory, Texas Instruments Incorporated, McKinney, TX 75069.

0018-9480/85/0900-0808$01.00 ©1985 IEEE

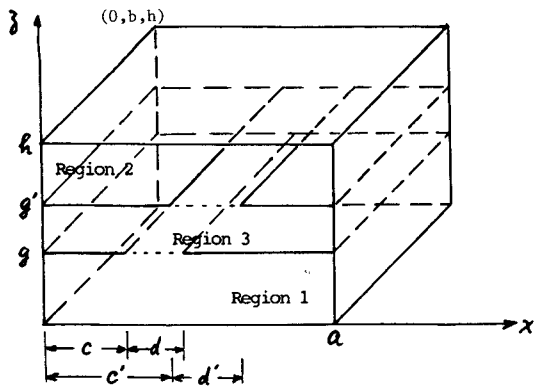

Fig. 2. Schematic diagram of three dielectric layer cavity. (a) Shielded two slotlines. (b) Shielded two striplines.

Following the examples illustrated here, more complicated transmission-line systems using striplines or slotlines can be analyzed by this technique.

In the presence of dielectric layers, the field distribution is confined to the neighborhood of the striplines or slotlines. Choosing sufficiently large waveguide sidewall spacings, open geometries can be approximated by shielded versions with negligible errors. Thus, the transverse modal analysis method is applicable to approximate the open geometry of slotlines and striplines.

The emphasis of this study is on the demonstration of achievable accuracy, not on the investigation of propagation characteristics. In addition to the comparison with known solutions, numerical convergence of the present application is also investigated. It is shown that the convergence characteristics of the computed resonant frequencies are similar to those observed in the scattering by irises or strips in rectangular waveguides.

II. Formulation

The basic formulation employs the transverse resonance concept and the modal analysis technique for rectangular waveguide discontinuities. Slotline and stripline cavities as shown in Figs. 1 and 2 are formed for computing the dispersion characteristics. Throughout this paper, the y-dependence of the field is either $\cos(\pi y/b)$ or $\sin(\pi y/b)$. At the cavity resonant frequency, the guided wavelength of the transmission-line system is equal to $2b$. Only uniform transmission lines are considered throughout this paper.

A. Finlines

The geometry of a finline parallel to the y-axis is shown in Fig. 1(a). Two electric walls are placed perpendicular to the y-axis at $y=0$ and $y=b$ to form a finline cavity. Consider that this cavity consists of two rectangular waveguide sections where the propagation is along the z-axis. These two waveguide sections are joined by a window at $z=g$ and are terminated by an electric wall at $z=h$, an electric or a magnetic wall at $z=0$, depending on the required geometry.

Derived equations in this subsection are applicable to finned rectangular waveguides and bilateral finlines. For a bilateral finline, a magnetic wall at $z=0$ produces the even-mode dispersion solution, while an electric wall yields the odd-mode results.

The fields in the two waveguide sections are expressed by the rectangular waveguide modal functions as follows [6].

For $g>z>0$ (region 1):

$$\boldsymbol{E}_t = \sum_n A_n \phi_n \begin{bmatrix} \sin \\ \cos \end{bmatrix} (\beta_n z) \tag{1a}$$

$$\boldsymbol{H}_t = j \sum_n A_n \hat{z} x \phi_n Y_n \begin{bmatrix} \cos \\ -\sin \end{bmatrix} (\beta_n z). \tag{1b}$$

For $h>z>g$ (region 2):

$$\boldsymbol{E}_t' = \sum_n B_n \phi_n \sin \beta_n'(h-z) \tag{2a}$$

$$\boldsymbol{H}_t' = -j \sum_n B_n \hat{z} x \phi_n Y_n' \cos \beta_n'(h-z). \tag{2b}$$

Here, the upper and lower functions are applied to the electric and magnetic wall at $z=0$, respectively, n is the compound modal index which represents two index numbers plus an index indicating the TE or TM mode, and ϕ_n is the normalized waveguide vectorial modal function. Note that the unprimed and primed quantities are employed to indicate the difference in the relative dielectric constants in regions 1 and 2, respectively. The wave admittance is related to the z-propagation constant β_n by $Y_n = \beta_n/\omega\mu$ for TE modes, and $Y_n = \omega\epsilon/\beta_n$ for TM modes, where ω is the angular frequency, μ and ϵ are the permeability and permittivity, respectively, and

$$\left.\begin{matrix} \beta_n \\ \beta_n' \end{matrix}\right\} = \left[k^2 \frac{\epsilon}{\epsilon'} (n\pi/a)^2 - (\pi/b)^2 \right]^{1/2}. \tag{3}$$

Let the electric field in the slot aperture be expressed by

$$\boldsymbol{E}_a = \sum_q C_q \Omega_q \tag{4}$$

where Ω_q is the vectorial basis function which may be represented by the modal functions of the slot equivalent waveguide, or simply by pulse functions. The boundary conditions at the slot plane are

$$\boldsymbol{E}_t = \boldsymbol{E}_t' = \begin{cases} \boldsymbol{E}_a, & \text{on the aperture} \\ 0, & \text{elsewhere} \end{cases} \tag{5}$$

$$\boldsymbol{H}_t = \boldsymbol{H}_t', \qquad \text{on the aperture.} \tag{6}$$

To enforce these boundary conditions, (1)–(4) are substituted into (5) and (6). Taking the scalar product of ϕ_n with the resultant equation obtained from (5) and integrating over the rectangular waveguide cross-section area yields

$$A_n \begin{matrix}\sin\\ \cos\end{matrix}(\beta_n g) = B_n \sin\left[\beta_n'(h-g)\right] = \sum_q C_q W_{qn} \tag{7}$$

where

$$W_{qn} = \int_{\text{slot}} \Omega_q \cdot \phi_n dS. \tag{8}$$

Taking the scalar product of Ω_q with the equation obtained from the boundary condition (6), integrating over the slot aperture, and combining with (7), we obtain a matrix equation given in the following form:

$$[M][C] = 0 \tag{9}$$

where

$$M_{pq} = \sum_n W_{qn} W_{pn} G_n \tag{10}$$

$$G_n = Y_n' \cot\left[\beta_n'(h-g)\right] + Y_n \left[\begin{matrix}\cot\\ -\tan\end{matrix}(\beta_n g)\right]. \tag{11}$$

In order to obtain a set of nontrivial coefficients, the determinant of the square matrix constructed from (9) must vanish. Since the determinant is a function of frequency and the finline guided wavelength is equal to $2b$, this requirement determines the cavity resonant frequencies and, hence, the dispersion characteristics of the finline. Substituting the resonant frequency back into (9), the slot field expansion coefficients and, hence, the cavity field can be computed from the above equations.

B. Shielded Microstrips

Similar to the finline, a cavity can be formed by placing two electric walls perpendicular to the shielded microstrip as shown in Fig. 1(b). This configuration can be employed to compute the dispersion characteristics of two shielded broadside-coupled striplines. The magnetic wall at $z = 0$ yields the even-mode solution while the electric wall at $z = 0$ applies to the odd-mode computation. Conveniently, (1) and (2) are used to represent the x- and y-components in regions 1 and 2, as before. Replacing the slot field representation by the stripline surface current density

$$\boldsymbol{J} = j\sum_q C_q \boldsymbol{v}_q \tag{12}$$

the pertinent boundary conditions are

$$\boldsymbol{E}_t = \boldsymbol{E}_t' \begin{cases} = 0, & \text{on the stripline} \\ & \text{elsewhere} \end{cases} \tag{13}$$

$$\hat{z}x\left(H_t - H_t'\right) = \begin{cases} 2\boldsymbol{J}, & \text{on the stripline} \\ 0, & \text{elsewhere.} \end{cases} \tag{14}$$

To enforce these boundary conditions, we first substitute (1), (2), and (12) into (13) and (14). Taking the scalar product of the resultant equation obtained from (13) with ϕ_n, then integrating over the waveguide cross section and taking the scalar product of the same equation with $\boldsymbol{v}_p$, then integrating over the stripline area, yields

$$A_n \left[\begin{matrix}\sin\\ \cos\end{matrix}(\beta_n g)\right] = B_n \sin\left[\beta_n'(h-g)\right] = U_n \tag{15}$$

$$\sum_n W_{pn} U_n = 0 \tag{16}$$

where U_n can be computed by combining (1), (2), (12), (14), and (15) and is given by

$$U_n = 2\sum_n C_q W_{qn}/G_n. \tag{17}$$

Here, G_n is given by (11), and W is defined by (8) with the slot field basis function replaced by the stripline surface current basis function. Upon substituting (17) into (16), we obtain a matrix equation given by the same form of (9) with the matrix elements defined by

$$M_{pq} = \sum_n W_{pn} W_{qn}/G_n. \tag{18}$$

After solving the determinant equation for the cavity resonant frequency, the current expansion coefficients and the cavity field distribution can be computed by substituting into (1), (2), (15), and (17).

C. Multiple Conductors with Multiple Dielectric Layers

The derivation shown above is applicable to simple finline or microstrip with only two dielectric layers (electric wall) or two broadside-coupled slotlines or striplines (electric wall for odd mode, magnetic wall for even mode). The same concept is also applicable to the general case of multiple conductors with multiple dielectric layers as shown in Fig. 2. The following equations are derived for two offset-coupled slotlines or two offset-coupled striplines.

With reference to Fig. 2(a) or (b), the fields in regions 1 and 2 can be expressed by the same equations as before. In region 3, where $g < z < g'$, the x- and y-components are written as

$$E_t'' = \sum_n \left[I_n \exp\left(-j\beta_n'' z\right) + R_n \exp\left(j\beta_n'' z\right)\right]\phi_n \tag{19a}$$

$$H_t'' = \sum \left[I_n \exp\left(-j\beta_n'' z\right) - R_n \exp\left(j\beta_n'' z\right)\right] Y_n \hat{z}x\phi_n \tag{19b}$$

where the double prime stands for region 3. All quantities in region 3 are defined the same as in region 2, except the prime is replaced by double prime.

Consider first the slotline case. The slot aperture electric field at $z = g$ is defined by (4), and at $z = g'$ by

$$E_a' = \sum_q C_q' \Omega_q'. \tag{20}$$

Enforcing the boundary conditions at $z = g$ and g', taking the scalar inner product of the electric field with the fields in the slotlines defined above, and a little mathematical

manipulation we obtain

$$I_p = \left[V_p \exp\left(j\beta_p'' g'\right) - V_p' \exp\left(j\beta_p'' g\right)\right] / \left\{2j \sin\left[\beta_p'(g'-g)\right]\right\} \quad (21a)$$

$$R_p = \left[V_p' \exp\left(-j\beta_p'' g\right) - V_p \exp\left(-j\beta_p'' g'\right)\right] / \left\{2j \sin\left[\beta_p''(g'-g)\right]\right\} \quad (21b)$$

$$V_p = \sum_q C_q W_{qp} \quad (21c)$$

$$V_p = \sum_q C_q' W_{qp}' \quad (21d)$$

where W and W' are defined as in (8) with integration limits and basis functions specified for the corresponding slotlines. Upon substituting these two equations into the magnetic-field equations obtained from the boundary conditions, a simple manipulation yields the following two matrix equations:

$$[R_{pq}][C_q] = [T_{pq}][C_q'] \quad (22a)$$

$$[R_{pq}'][C_q'] = [T_{pq}'][C_q] \quad (22b)$$

where

$$R_{pq} = \sum_n W_{pn} W_{qn} G_n \quad (23a)$$

$$R_{pq}' = \sum_n W_{pn}' W_{qn}' G_n' \quad (23b)$$

$$T_{pq} = \sum_n W_{pn} W_{qn}' F_n \quad (23c)$$

$$T_{pq}' = \sum_n W_{pn}' W_{qn} F_n \quad (23d)$$

$$G_n = Y_n \left[\begin{matrix}\cot \\ -\tan\end{matrix}(\beta_p g)\right] + Y_n'' \cot\left[\beta_n''(g'-g)\right] \quad (24a)$$

$$G_n' = Y_n' \cot\left[\beta_n'(h-g')\right] + Y_n' \cot\left[\beta_n''(g'-g)\right]. \quad (24b)$$

Eliminating $[C_q']$ in (22), we obtain the matrix equation given by the same form of (9) with

$$[M_{pq}] = [R_{pq}] - [T_{pq}][R_{pq}']^{-1}[T_{pq}']. \quad (25)$$

The nontrivial solution of $[C_q]$ and, hence, $[C_q']$ can be computed by setting the determinant of (25) equal to zero as in the previous finline and microstripline cases.

Equations similar to (22)–(25) can be derived for the two offset-coupled striplines as shown in Fig. 2(b). In this case, the slot aperture electric fields of (4) and (20) are replaced by the surface current densities of (12) and

$$J' = \sum_q J_q' \mathbf{v}_q'. \quad (26)$$

Using the same derivation as in the shielded microstrip case, we obtain (22) and (25), provided that G_n and G_n' in (23a) and (23b) are replaced by G_n'/D_n and G_n/D_n, respectively, and F_n in (23c) and (23d) is replaced by $-F_n/D_n$, where

$$D_n = G_n G_n' - F_n^2.$$

After the resonant frequency is determined, the characteristic impedance can be computed by the known field distribution, which requires the solution of (21). For the stripline case, (21) is replaced by the following form:

$$I_n = \left[U_n \exp\left(j\beta_n'' g'\right) - U_n' \exp\left(j\beta_n'' g\right)\right] / \left[2j \sin \beta_n''(g'-g)\right] \quad (27a)$$

$$R_n = \left[U_n' \exp\left(-j\beta n'' g\right) - U_n \exp\left(-j\beta_n'' g\right)\right] / \left[2j \sin \beta_n''(g'-g)\right] \quad (27b)$$

where

$$U_n = -j \sum_q \left(G_n' J_g W_{qn} + F_n J_q W_{qn}\right) / D_n \quad (28a)$$

$$U_n' = -j \sum_q \left(G_n J_q' W_{qn}' + F_n J_q W_{qn}\right) / D_n. \quad (28b)$$

W and W' are defined by (8) with the slot field basis function replaced by the stripline surface current basis function and the integration limits taken over the corresponding stripline. These equations can be used to specify the field distribution at the given resonant frequency. Note that the convention of the magnetic or electric wall at $z = 0$ remains valid for the above equations.

III. Modal Functions and Basis Functions

The rectangular waveguide vectoral modal functions for TE and TM modes are given by Marcuvitz [6] in the following normalized expressions:

$$\begin{bmatrix}\phi_{1n} \\ \phi_{2n}\end{bmatrix} = N_n \left[\hat{x}\begin{pmatrix}1/b \\ n/a\end{pmatrix} E_{xn} + \hat{y}\begin{pmatrix}-n/a \\ 1/b\end{pmatrix} E_{yn}\right] \quad (29)$$

$$N_n = \left\{2\delta_n / ab / \left[(n/a)^2 + (1/b)^2\right]\right\}^{1/2} \quad (30a)$$

$$\begin{bmatrix}E_{xn} \\ E_{yn}\end{bmatrix} = \begin{matrix}\cos \\ \sin\end{matrix}(n\Pi x/a) \begin{matrix}\sin \\ \cos\end{matrix}(\Pi y/b) \quad (30b)$$

$$\delta_n = \begin{cases}1 \text{ if } n = 0 \\ 2 \text{ if } n \neq 0\end{cases}. \quad (30c)$$

These expressions have been specified for the y-dependence as shown. Both TE and TM are referred to the z-propagating modes and are suitable for the present application.

In general, the basis functions in (4), (12), (20), and (26) have both the x- and y-components since the general propagating modes in a slotline or a stripline are hybrid modes. However, the dominant slotline mode is a TE mode and the dominant stripline mode is a quasi-TEM mode. Thus, the fundamental mode requires only the x-component of the slot field or the y-component of the stripline current.

For a narrow slot or strip, single field or current component representation is sufficient not only for the dominant mode, but also for the next higher order mode. Also, only one or two terms in the basis functions are adequate to represent the slot field or the strip current density, and the solution obtained is sufficiently accurate for many engineering applications. The following general form can be

used for all cases considered above:

$$\Omega_q = \hat{x}C_{xq}e_{xq} + \hat{y}C_{yq}e_{yq} \tag{31}$$

$$v_q = \hat{x}C'_{xq}j_{xq} + \hat{y}C'_{yq}j_{yq} \tag{32}$$

$$\begin{bmatrix} e_{xq} \\ e_{yq} \end{bmatrix} = \begin{matrix} \cos \\ \sin \end{matrix} [q\pi(x-c)/d] \begin{matrix} \sin \\ \cos \end{matrix} (\pi y/b) \tag{33a}$$

$$\begin{bmatrix} j_{xq} \\ j_{yq} \end{bmatrix} = \begin{matrix} \sin \\ \cos \end{matrix} [q\pi(x-c)/d] \begin{matrix} \sin \\ \cos \end{matrix} (\pi y/b). \tag{33b}$$

The primed basis functions are given by the same expressions as above except that c and d are replaced by c' and d', respectively.

For a narrow slotline or stripline, the pulse basis functions are quite accurate and can be used for practical computation. The pulse basis function is defined

$$\Pi q(x, x_q, \Delta) = \begin{cases} 1, & x_q - \Delta/2 < x < x_q + \Delta/2 \\ 0, & \text{elsewhere} \end{cases} \tag{34}$$

where x_q is an arbitrary point on the slot aperture or the strip conductor. Equation (34) is used to replace the first factor in the right-hand side of (33).

IV. Numerical Results

Based on the above formulation and the specified basis functions, dispersion characteristics of finned rectangular waveguides, shielded bilateral finlines, microstrip, and shielded coupled striplines are computed for comparison with various published results. Favorable comparisons verify the validity and the usefulness of the transverse modal analysis technique. Trigonometric basis functions are used to compute the following dispersion results by the transverse modal analysis (TMA) method unless otherwise stated. All the frequencies listed in the following are understood in gigahertz and lengths in inches.

A. Finned Rectangular Waveguides

A finned rectangular waveguide is a finline without the dielectric substrate as shown in Fig. 1(a). Numerical solutions can be computed from the equations derived in Section II-A with identical dielectric constants. Waveguide dimensions of $a = 1$ in by $h = 2$ in and the finlines located at the middle of the waveguide are chosen for the present example.

Consider first the half-width slot where $d = 0.5$ in. The computed dominant mode cutoff wavelengths with slot mode to the waveguide mode ratios equal to 1/2, 1/4, and 3/4 are shown in Fig. 3(a). The proper mode ratio is 1/2. The noncontributing modes by geometric symmetry are kept for computer programming convenience. Keeping the waveguide mode number equal to 30, the cutoff wavelength versus the number of slot modes is plotted in Fig. 3(b). These plots are similar to the equivalent susceptance of a waveguide iris computed by the modal analysis. Similar convergence characteristics are observed using the pulse basis functions, but the rate of convergence is slower. Note that the computed cutoff wavelengths are independent of the cavity length chosen in the computation.

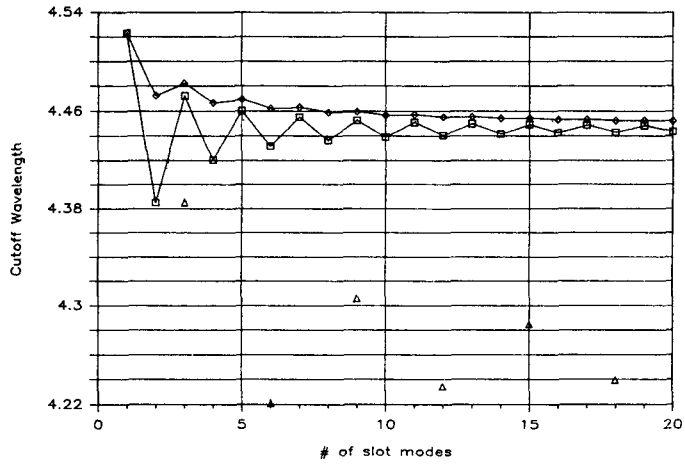

(a)

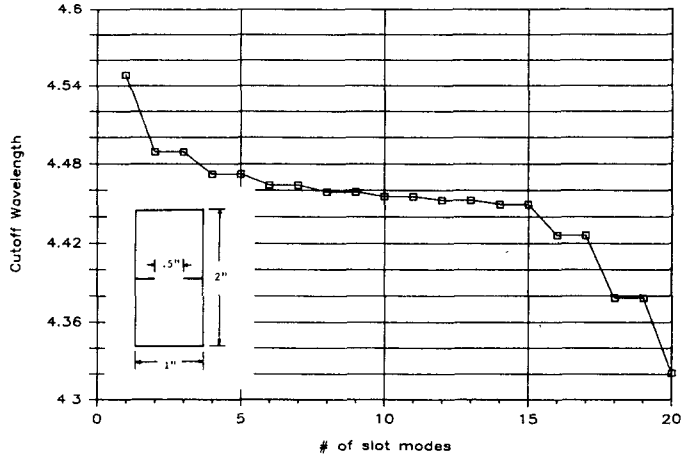

(b)

Fig. 3. Computed cutoff wavelength for a finned rectangular waveguide. (a) Constant slot to waveguide mode ratio. □□□ ratio = 1/2, ◇◇◇ ratio = 1/4, △△△ ratio = 3/4. (b) 30 waveguide modes.

TABLE I
Comparison of the Finned Rectangular Waveguide Cutoff Wavelengths

	TMA			TLM	TR
Slot Width	Trigonometric	Pulse	Single BF		
1/2	4 4503	4 4583	4 5233	4 4385	4 4464
1/4	5 1950	5 2115	5 2488	5 1760	5 1867
1/16	6 5961	6 6227	6 5946	6 5703	6 5876

Waveguide dimensions: 1″ by 2″.

Computed cutoff wavelengths of various finned rectangular waveguides are tabulated in Table I. Proper mode ratios and a sufficient number of basis functions are employed by the TMA method. These results compare favorably with those computed by Shih and Hoefer [7] using the transmission-line matrix (TLM) technique and by Hoefer [8] using the quasi-static transverse resonant (TRT) method.

Numerical experiments show that sufficient accurate results are obtained by adding one more basis function for each incremental slot width of 0.01 wavelength. For a narrow slot with slot width $d = 1/16$, shown in Table I,

TABLE II
COMPUTED CUTOFF FREQUENCIES OF FINLINE #1

Slot Width	Slab Thickness	TMA Domt Mode	TMA 2nd Mode	TLM Domt Mode	TLM 2nd Mode
1/8	1/8	1 5202	3 8794	1 514	3 965
1/8	1/4	1 4117	3.4370	1 415	3 486
1/8	1/2	1 3807	2 8625	1.359	2 890
1/2	1/8	2 3041	5 5683	2.306	5 594
1/2	1/4	2 1364	5 1485	2.125	5.144
1/2	1/2	1 9897	4.4590	1 987	4 450

only one basis function is required to obtain the comparable accuracy. Using only one basis function, the computed cutoff wavelength is equal to 6.5946 as compared to 6.5899 using nine basis functions.

B. Bilateral Finlines

The bilateral finline is shown in Fig. 2(a) with $c = c'$ and $d = d'$. The odd-mode dispersion characteristics are identical to that in a shielded slotline. Bilateral finlines have been investigated by Shih and Hoefer [9], who employed the TLM method, and Schmidt and Itoh [10], who employed the spectral-domain (SD) method. The following two configurations are considered here.

Finline #1

Waveguide dimensions	1.0 by 2.0 in,
Dielectric slab	relative dielectric constant = 2.2, thickness = 0.5 in, 0.25 in, and 0.125 in,
Slot width	0.5 in and 0.125 in.

Finline #2

Waveguide dimensions	0.14 in by 0.28 in,
Dielectric slab	relative dielectric constant = 3.0, thickness = 0.00492 in,
Slot width	0.019685 in.

Tabulated in Table II are the computed cutoff frequencies of the bilateral finline #1. Cutoff frequencies can be computed by setting b extremely large compared to a. Both the dominant and second-order mode cutoff frequencies computed by the TMA method compare favorably with those computed by TLM shown in the same table.

The effective dielectric constants of the dominant and second-order modes in finline #2 have been computed by Schmidt and Itoh using the SD method [10]. Their results are tabulated in Table III with those computed by the TMA method. Excellent agreement between these two sets of computed results verify the validity of these two methods. Note that the square root of the effective dielectric constant is equal to the resonant wavelength divided by $2b$.

To illustrate the dielectric slab effect on the convergence characteristics, computed effective dielectric constants of the dominant mode in finline #2 versus the maximum slot mode index are shown in Fig. 4, where the proper mode ratio is 1/8. Note that the convergence is about the same as in the absence of the dielectric slab. Plotted in Fig. 5 are the same dispersion results computed by the pulse basis functions. Computed results by the pulse basis functions converge slower than, but approach the same solutions as computed by the trigonometric basis functions.

TABLE III
COMPUTED EFFECTIVE DIELECTRIC CONSTANTS OF FINLINE #2

Dominant Mode Freq	Dominant Mode TMA	Dominant Mode SD	Second Order Mode Freq	Second Order Mode TMA	Second Order Mode SD
14.100	0 2737	0.250	47 645	0 0240	0.00
21.621	0 8278	0 828	50.893	0 1494	0 157
29 262	1 0168	1 026	55 290	0.2848	0 297
37 375	1 1081	1.120	60 928	0.4170	0.423
54.038	1 1927	1 200	74.807	0.6224	0 631
62.906	1.2182	1 225			

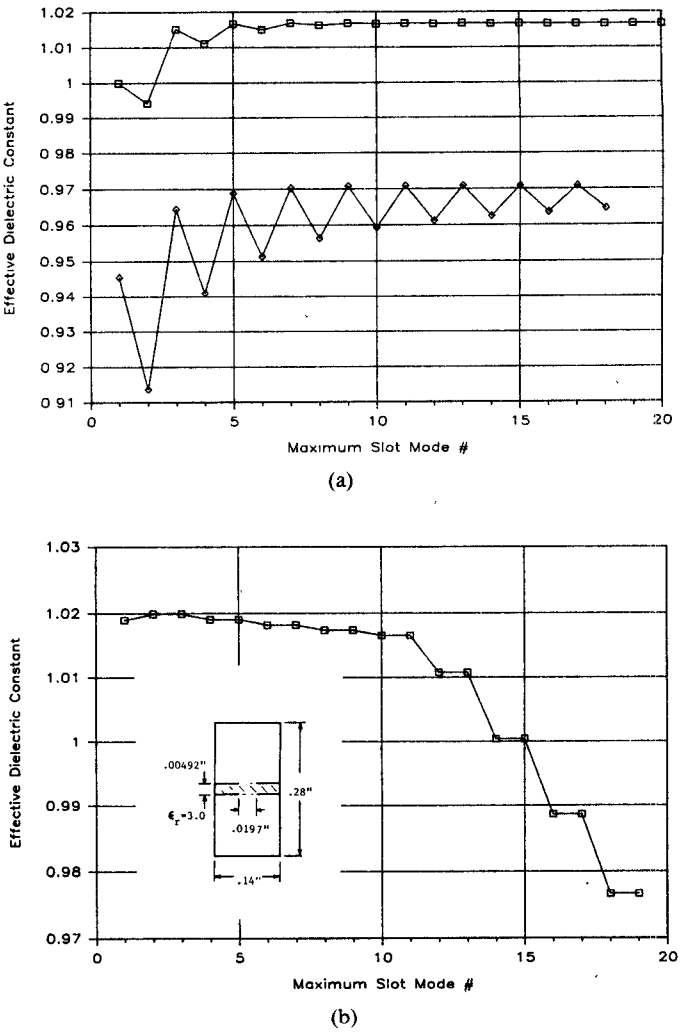

Fig. 4. Computed effective dielectric constant for finline #2 at 29.26 GHz. (a) Constant mode ratio. □□□ ratio = 1/8, ◇◇◇ ratio = 1/4. (b) 80 waveguide modes.

C. Shielded Microstrips

Dispersion characteristics of shielded microstrips have been investigated by Daly [11] using the finite-element

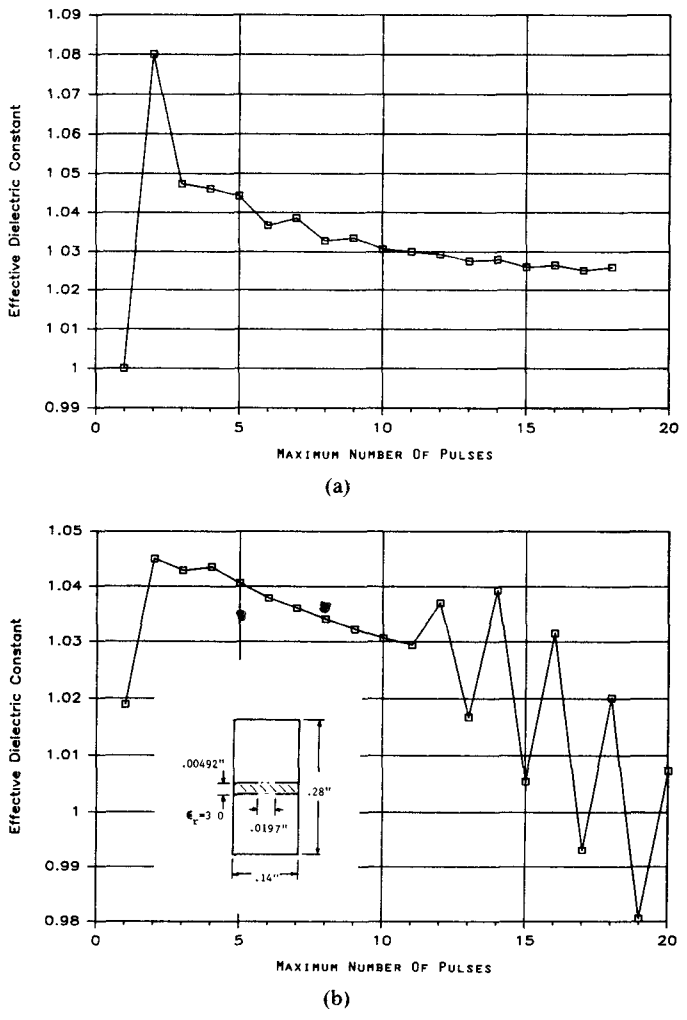

Fig. 5. Effective dielectric constant of finline #2 at 29.26 GHz computed by pulse-basis function. (a) Pulse to waveguide mode ratio = 1/8. (b) 80 waveguide modes.

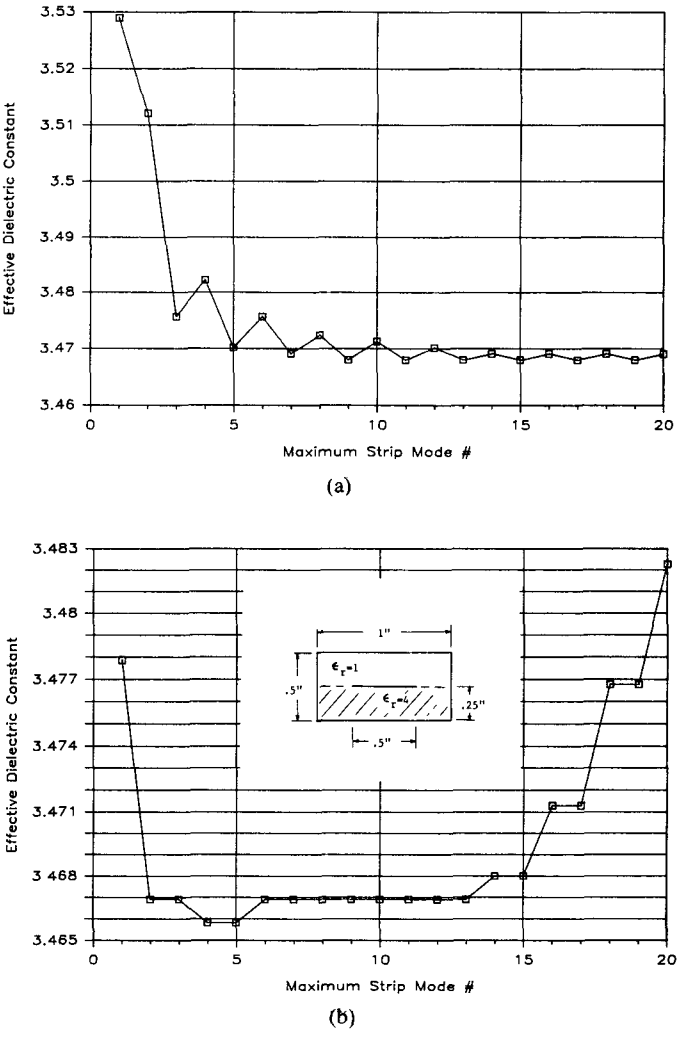

Fig. 6. Computed effective dielectric constant of a shielded microstrip at 6.34 GHz. (a) Strip to waveguide mode ratio = 1/2. (b) 30 waveguide modes.

TABLE IV
COMPARISON OF COMPUTED EFFECTIVE DIELECTRIC CONSTANT OF A SHIELDED MICROSTRIP.

Quasi-TEM Mode			Waveguide Mode		
Freq	TMA	Finite Element	Freq	TMA	Finite Element
3 411	2 9934	2 964	6 440	0 8398	0 841
4 402	3 1952	3 185	7 553	1 8053	1 090
6 337	3 4681	3 455	9 495	1 5452	1 536
8 819	3 6555	3 635	12 099	1 9422	2 081
10 201	3 7187	3 712	13 288	2 1916	2 340

Stripline width = 0.5". Waveguide dimensions: 1.0" by 0.5". Dielectric slab: thickness = 0.25". Relative constant = 4.0.

method. The effective dielectric constants of the dominant mode (quasi-TEM mode) and a higher order mode computed by the finite-element method and by the transverse modal analysis method are shown in Table IV. Observe that these values, including both the quasi-TEM and a higher order mode, computed by two different methods agree very well with each other.

Depicted in Fig. 6 are the computed effective dielectric constant versus the strip modal index number for the example microstrip at the frequency approximately equal to 6.34 GHz. The proper mode ratio is 1/2. The convergence is similar to that for finlines except that the computed effective dielectric constant follows a decreasing trend as the strip mode number increases.

D. *Broadside-Coupled Striplines*

Using the equations derived in either Section II-B or II-C, one can compute the dispersion characteristics of shielded two broadside-coupled striplines. When the equations derived in Section II-B are employed, the electric wall equations are applied to the odd modes and the magnetic wall equations to the even modes.

Computed effective dielectric constants of both even and odd modes are tabulated in Tables V and VI for comparison with those computed by Kawano [12] and Wu [13]. The results of Kawano and Wu are computed by the spectral-domain technique with no sidewalls in the geometry. However, two sidewalls are required using the transverse modal analysis method. The sidewall effects on the odd mode is negligible if the sidewall spacing is equal to 10 stripline widths or greater. In the case of the even mode, the sidewall spacing must be equal to or greater than 20 stripline widths. Thus, a 20-stripline width sidewall spacing

TABLE V
COMPARISON OF COMPUTED EFFECTIVE DIELECTRIC CONSTANTS OF TWO SHIELDED BROADSIDE STRIPLINES

Even Mode				Odd Mode			
Freq	TMA	Kawano	Wu	Freq	TMA	Kawano	Wu
2.664	1 2269	1 224	1 244	2 151	1 8818	1 877	1 916
6 647	1 2317	1 234	1 253	5 341	1 9077	1 900	1 926
8 846	1 2365	1 241	1 258	7 097	1 9210	1 913	1 939
13 197	1 2499	1 246	1 271	10 585	1 9430	1 935	1 958
25 636	1 3249	1 331	1 353	20 888	1 9956	1 989	2 006
29 178	1 3358	-------	1 386	27 647	2 0252	2 019	2 040

Waveguide dimension: 1.1969″ by 0.2992″. Dielectric slab: thickness = 0.02992″. Relative constant = 2.32. Stripline width = 0.05984″.

TABLE VI
COMPARISON OF COMPUTED EFFECTIVE DIELECTRIC CONSTANTS OF TWO SHIELDED BROADSIDE STRIPLINES

Even Mode				Odd Mode			
Freq	TMA	Kawano	Wu	Freq	TMA	Kawano	Wu
2.064	2 045	2 03	2 08	2 281	6.694	6 68	6 78
4 111	2 061	2 08	2 15	5 647	6.826	6 78	6 89
10 061	2 151	2 16	2 15	11 133	7 026	6 97	7 09
18 711	2 487	2 45	2 55	21 761	7 355	7 27	7 42
27 947	3 097	2 91	3 05	27 597	7 516	7 41	7 59

Waveguide dimension: 0.4724″ by 0.2992″. Dielectric slab: thickness = 0.02992″. Relative constant = 9.6. Stripline width = 0.05984″.

TABLE VII
COMPARISON OF COMPUTED EFFECTIVE DIELECTRIC CONSTANTS OF TWO OFFSET COUPLED STRIPLINES

Odd Mode			Even Mode		
Freq	TMA	Wu	Freq	TMA	Wu
4 025	2 150	2 142	4 155	2 017	2 026
10 059	2 151	2 144	10 389	2 017	2 026
20.109	2 153	2.147	20 778	2.017	2 027
29 780	2 155	2.150	30 780	2 017	2 029
39 396	2 157	2 153	39 573	2.017	2 029
20 573*	0 0	------			
23 000*	0 412	0 375			
29,096*	1 029	1 050			
39 000*	1 479	1 530			

Offset = 0.05″. Waveguide dimension: 2.0″ by 0.134″. Dielectric slab: thickness = 0.01″. Relative constants = 2.0 and 2.2. Stripline width = 0.1″.

*Higher order modes.

is used to compute the TMA results shown in Tables V and VI.

Observe that the effective dielectric constants computed by the TMA method fall between the results computed by Kawano and Wu. The data of Kawano and Wu are obtained from interpolation of plotted curves. It is interesting to note that identical TMA results are obtained using the equations of Sections II-B and II-C.

E. Offset-Coupled Striplines

A generalized geometry of two offset-coupled striplines as shown in Fig. 2(b) is quite important in the coupler design. Its propagation characteristics have not been reported in the open literature. Using the equations derived in Section II-C, the dispersion characteristics of two offset-coupled striplines can be computed. The computed effective dielectric constants of two dielectric geometries are tabulated in Table VII. Also tabulated in Table VII is the dispersion results computed by Wu [13] using the spectral-domain method as in the broadside-coupled striplines.

Again, excellent agreement is observed for both even- and odd-mode solutions between these two computational methods.

V. CONCLUSION

The transverse modal analysis has been demonstrated as a useful technique for computing the dispersion characteristics of several transmission-line systems, such as finned rectangular waveguides, finlines, shielded microstrips and strips, and shielded two-coupled slotlines and strips. Numerical results computed by the transverse modal analysis method are in close agreement with those computed by the transmission-line matrix, transverse resonance, finite-element, and spectral-domain methods. The achievable accuracy is beyond engineering requirements. Both the dominant mode and higher order modes have been examined.

Although most of the computation used trigonometric basis functions, it is shown that comparable accuracy is achieved by the pulse basis functions, especially for narrow slotlines or striplines. However, in the case of broad slots or strips, the computed results using the pulse functions are less accurate and converge slower than those using trigonometric functions.

Also, it is demonstrated that the convergence is not affected by the presence of a dielectric slab. It is shown that only a small number of basis functions are required for narrow striplines or slotlines. Therefore, the transverse modal analysis is well suited for printed circuit transmission-line analysis.

In addition to the transmission-line systems discussed above, the transverse modal analysis can be applied to other complicated configurations. The dispersion characteristics of a slot coupled to a parallel stripline can be computed by a modification of (22)–(24). Multiple layers of dielectric slabs transmission-line systems can be investigated by extension of the technique formulated here.

REFERENCES

[1] S. Lee, W. Jones, and J. Campbell, "Convergence of numerical solutions of iris-type discontinuity problems," *IEEE Trans. Microwave Theory Tech.*, vol. MTT-19, pp. 528–536, June, 1971.

[2] R. Mittra, T. Itoh, and T.-S. Li, "Analytical and numerical studies of the relative convergence phenomenon arising in the solution of an integral equation by the moment method," *IEEE Trans. Microwave Theory Tech.*, vol. MTT-20, pp. 96–104, Feb. 1972.

[3] J. Collins and P. Daly, "Orthogonal mode theory of single ridge waveguide," *J. Electron. Contr.*, vol. 17, 1st series, 7–12, pp. 121–129, 1964.

[4] J. Montgomery, "On the complete eigenvalue solution of ridged waveguide," *IEEE Trans. Microwave Theory Tech.*, vol. MTT-19, pp. 547–555, 1981.

[5] R. Sorrentino and T. Itoh, "Transverse resonance analysis of finline discontinuities," in *IEEE MTT-S Int. Symp. Dig.*, 1984, pp. 414–416.

[6] N. Marcuvitz, *Waveguide Handbook*. New York: McGraw-Hill, 1950, ch. 5.

[7] Y.-C. Shih and W. Hoefer, "The accuracy of TLM analysis of finned rectangular waveguides," *IEEE Trans. Microwave Theory Tech.*, vol. MTT-28, pp. 743–746, 1980.

[8] W. Hoefer, "Fin-line design made easy," in *IEEE MTT-S Int. Microwave Symp. Dig.*, June 1978, pp. 27–29.
[9] Y.-C. Shih and W. Hoefer, "Dominant and second order mode cutoff frequencies in fin lines calculated with a two-dimensional TLM program," *IEEE Trans. Microwave Theory Tech.*, vol. MTT-28, pp. 981–985, 1980.
[10] L-P. Schmidt and T. Itoh, "Spectral-domain analysis of dominant and high order modes in fin-line," *IEEE Trans. Microwave Theory Tech.*, vol. MTT-28, pp. 981–985, 1980.
[11] P. Daly, "Hybrid-mode analysis of microstrip by finite-element methods," *IEEE Trans. Microwave Theory Tech.*, vol. MTT-19, pp. 19–25, 1971.
[12] K. Kawano, "Hybrid-mode analysis of a broadside-coupled microstrip line," *Inst. Elec. Eng.*, vol. 131, pt. H, pp. 21–24, 1984.
[13] K. Wu, private communication.

✠

Hung-Yuet Yee (SM'70) received the Ph.D. degree in electrophysics from the Polytechnic Institute of New York in 1968.

From July 1963 to February 1966, he was a Research Associate with the University of Alabama Research Institute, Huntsville, AL. From July 1968 to August 1971, he was a Senior Research Associate and Assistant Professor with the University of Alabama in Huntsville. In August 1971, he jointed the staff of Texas Instruments, Inc., and was assigned to the Antenna Laboratory. Since 1979, he has been a Senior Member of the Technical Staff.